ISSN 1024-8560, Atmospheric and Oceanic Optics, 2023, Vol. 36, No. 4, pp. 337–347. © The Author(s), 2023. This article is an open access publication.
Russian Text © The Author(s), 2023, published in Optika Atmosfery i Okeana.

ATMOSPHERIC RADIATION, OPTICAL WEATHER, AND CLIMATE

Application of the CHIMERE-WRF Model Complex to Study the Radiative Effects of Siberian Smoke Aerosol in the Eastern Arctic

I. B. Konovalov[a, *], N. A. Golovushkin[a], T. B. Zhuravleva[b], I. M. Nasrtdinov[b], V. N. Uzhegov[b], and M. Beekmann[c]

[a] *Federal Research Center, Gaponov-Grekhov Institute of Applied Physics, Russian Academy of Sciences, Nizhny Novgorod, 603950 Russia*

[b] *V.E. Zuev Institute of Atmospheric Optics, Siberian Branch, Russian Academy of Sciences, Tomsk, 634055 Russia*

[c] *Laboratoire Interuniversitaire des Systèmes Atmosphériques UMR 7583, CNRS, Faculte Sci. & Tech., 61 Ave. General de Gaulle, Creteil Cedex, 94010 France*

**e-mail: konov@ipfran.ru*

Received September 15, 2022; revised October 25, 2022; accepted November 28, 2022

Abstract—We describe a computational technology for studying the effects of the aerosol-radiation interaction and calculating regional estimates of the direct (DRE) and semidirect radiative effects (SDRE) of biomass burning (BB) aerosol based on simulations with the CHIMERE chemistry transport model coupled with the WRF meteorological model. The technology was applied to numerical studying the radiative effects of Siberian biomass burning aerosol in the eastern Arctic in the period of July 16–31, 2016. The model simulations show that Siberian smokes, on the whole, had a significant cooling effect on the atmosphere in the eastern Arctic in that period due to the DRE, the value of which at top of the atmosphere was, on average, -6.0 W m^{-2}, being minimal over the snow-ice cover of the ocean (-1.2 W m^{-2}). At the same time, the contribution of the Siberian BB aerosol DRE to the radiative balance of the Arctic atmosphere is found to be offset to a certain extent by the SDRE, which is positive (2.0 W m^{-2}), on average. The SDRE is formed as a result of the multihour aerosol effect on meteorological processes and plays the most important role over the snow-ice Arctic covers, where it exceeds the DRE in absolute value. It has been shown that the SDRE of Siberian BBA in our numerical experiments is mainly due to scattering (rather than absorption) of radiation by aerosol particles.

Keywords: aerosol, smoke, chemistry transport model, aerosol-radiation interaction

DOI: 10.1134/S1024856023040085

INTRODUCTION

Atmospheric aerosol introduces a significant contribution to the radiation balance of the Arctic atmosphere, thereby influencing the rapid climate change in this region [1]. In the general case, aerosol impacts the radiative fluxes through radiative effects, differing by their origin, namely:

— The aerosol–radiation interaction (ARI), comprising the direct radiative effect (DRE) [2], which is caused directly by absorption and scattering of radiation by aerosol particles, and semidirect radiative effect (SDRE) [3], which develops as a result of the DRE influence on thermal structure of the atmosphere and on clouds.

— Aerosol–cloud interaction [4], associated with the effect of condensation nuclei on cloud formation and cloud dynamics.

— Radiative effect acting to reduce the snow-ice surface albedo as a consequence of deposition of absorbing aerosol components, and primarily black and brown carbon, on the surface [5].

Landscape fires in northern Eurasia, most severe in Siberia, are known to be one of the main sources of aerosol in the Arctic during the warm period of the year [6]. However, in contrast to radiative and climatic effects of anthropogenic aerosol, which are the subject of many studies, similar effects of biomass burning (BB) BB aerosol (BBA) are still poorly understood. Among the studies of the BBA radiative effects in the Arctic, we can mention those in which local estimates of biomass burning aerosol DRE were obtained using data of measurements [7–9]. The authors of work [1], carried out using a few global chemistry transport models (CTMs), estimated different radiative effects both due to anthropogenic aerosol and to smokes in the Arctic, and sources from a few regions in the Northern Hemisphere were separately considered. Certain model estimates of the BBA radiative effects were published previously [10–14] as a minor part of research into global-scale ARI.

The large differences between BBA radiative effects in the Arctic obtained using different models within an ensemble of numerical experiments [1, 12] indicate

the high uncertainties of the model estimates. In turn, these uncertainties stem from well-known uncertainties existing in model representations of the sources [6, 14, 15], atmospheric conversions, and BBA optical properties [16–19].

One of the promising approaches to studying numerous factors, which determine the BBA optical and radiative properties and are responsible for uncertainties in model estimates of BBA radiative effects under the conditions of a specific territory, is based on application of regional three-dimensional models, in which the totality of meteorological and chemical processes in the lower atmosphere is taken into account with a high degree of detail, atypical for global and climate models. The meteorological chemical model WRF-CHEM [20–22], as well as the model complex relying on CTM CHIMERE coupled with the WRF model [15–17, 23] was applied within this approach in a number of studies. An important feature of the WRF-CHEM model is the "online" method for calculating the transport and chemical conversions of aerosols and gases, within which these processes are simultaneously calculated with meteorological characteristics and affect them through disturbances of radiative fluxes and/or concentrations of condensation nuclei. Due to this feature, the application of WRF-CHEM to estimation of the aerosol DRE and SDRE separately is difficult because the online calculated radiative fluxes are simultaneously determined by both ARI effects.

On the other hand, the CHIMERE CTM was originally designed for the so-called "offline" simulations, evaluating the chemical processes and transport using preset characteristics of the meteorological processes [24]. Simulations CHIMERE does not provide radiative flux simulations; therefore, CHIMERE cannot calculate any radiative effects of aerosol when used jointly with WRF in offline mode. However, the radiative effects of different aerosol types can now be studied with CHIMERE updated to a new version, enabling both online and offline simulations of the aerosol transport and conversions [25–27].

The purpose of this work is to study how the CHIMERE-WRF model complex can be used to study the ARI of Siberian BBA in the eastern Arctic and to separately estimate DRE and SDRE. Other BBA radiative effects (including the effects of the aerosol–cloud interaction) are beyond the scope of this work.

Our research is based on the development and subsequent application of original method (computational technology) for the DRE and SDRE calculation. In contrast to similar methods, applied previously in WRF-CHEM-based studies [20, 21], we suggest rejecting the assumption that the occurrence of BBA SDRE is uniquely related to the presence of black carbon (or other absorbing components) in BBA composition, which allows estimation of not only the contribution of absorption, but also of scattering of radiation by aerosol particles to SDRE. Numerical experiments performed within this work cover a relatively short period (the second half of July 2016), when severe wild fires occurred in Western Siberia.

1. COMPUTATIONAL TECHNOLOGY FOR BIOMASS BURNING AEROSOL DRE AND SDRE ESTIMATION

The initial task of the suggested computational technology is to estimate the ARI effect (Φ_{ARI}) at the top and bottom of the atmosphere. The Φ_{ARI} values in a given model cell at a given time are assumed to be related to the model-calculated radiative fluxes at the top or bottom of the atmosphere by the following general formula [19]:

$$\Phi_{ARI} = F^{\downarrow all} - F^{\downarrow bg} - (F^{\uparrow all} - F^{\uparrow bg}), \quad (1)$$

where F are the total radiative fluxes in the UV, visible, and thermal spectral ranges at a given atmospheric level; the superscript "all" indicates the fluxes in the calculation assuming that the atmospheric aerosol content is determined by all main sources, including BBA sources (i.e., landscape fires), "bg" marks the fluxes calculated without BBA sources; and arrows indicate the flux directions.

It is important to note that the differences of the fluxes F^{all} and F^{bg} are generally determined not only by scattering and absorption of radiation by BBA particles (i.e., not only by DRE), but also by differences in other atmospheric parameters which affect the propagation of solar radiation in the atmosphere. Those differences between F^{all} and F^{bg}, arising due to the redistribution of the solar radiative energy inside the atmosphere by the BBA particles, determine SDRE [3], which is of special interest in the context of the present work. In other words, Φ_{ARI} comprises both BBA DRE and BBA SDRE, the values of which are denoted below as Φ_d and Φ_{sd} (here, d stands for direct; and sd for semidirect). In contrast to DRE, which appears (disappears) at a given point in the atmosphere almost instantaneously after a smoke plume appears (disappears) at this point, the SDRE formation, by definition, is long-lasting (accumulative) in character. Based on these considerations, within this work the Φ_{ARI} estimate, like the Φ_{sd} estimate, is assumed to be a function of the calculational parameter τ, which is taken into account in numerical experiments and quantifies how long does the atmosphere adapt to the BBA radiative effect:

$$\Phi_{ARI}(\tau) = \Phi_d + \Phi_{sd}(\tau). \quad (2)$$

Based on Eq. (2), the Φ_d can be estimated as the value of Φ_{ARI} at $\tau = 0$:

$$\Phi_d = \Phi_{ARI}(0), \quad (3)$$

and $\Phi_{sd}(\tau)$, as the difference $\Phi_{ARI}(\tau) - \Phi_{ARI}(0)$.

Since all parameters included in Eqs. (2) and (3), vary in space and time (being independent of spatiotemporal fields of aerosol sources and meteorological parameters), it is useful to average their values over quite a long period of time (a week or longer) and over quite a large region (with characteristic sizes of a thousand of kilometers or more). In this work, it is assumed that Φ_{ARI} and Φ_{sd}, thus averaged, relatively rapidly approach (on timescale of a few hours) to certain limiting values as τ increases; therefore, their reasonable estimates, characterizing these radiative effects in the real atmosphere, can be obtained for a preset finite τ. The validity of this assumption is confirmed (at least partly) by numerical experiments presented in section 3.

The radiative fluxes are calculated by WRF and are its standard output parameters. To account for changes in these values as a result of aerosol–radiation interaction, CHIMERE transfers to WRF the values of key aerosol optical characteristics, including aerosol optical depth (AOD), single scattering albedo (SSA), and asymmetry factor (AF), for a number of wavelengths covering UV, visible, and near-IR ranges in online mode at each integration step (usually taken to be 10 min) and for each three-dimensional grid cell [27]. It is noteworthy that the offline mode makes it possible to calculate the changes in the atmospheric composition after disabling BBA sources for fixed meteorological parameters, which is required for the DRE estimation.

Thus, the computational technology developed for the DRE and SDRE calculations comprises a combination of online and offline simulations that can be split into two stages.

During the first (preparatory) stage (Fig. 1a), the software performs a series of successive 6-hour WRF-based simulations, covering the period under consideration (16 days in our work), using "cold" start (i.e., using global data as initial conditions) for each of the successive simulations. The six-hour interval is equal to the time step in the global reanalysis data used in the simulations, and can be reduced. During this stage, the software performs in parallel a series of CHIMERE-based offline simulations (with meteorological data available from WRF) with and without accounting for emissions from fires. The series of the CHIMERE simulations starts with global (climatological) initial conditions, and every next six-hour calculation uses results from preceding model run as initial conditions.

During the second stage, the software performs a series of online simulations (Fig. 1b) taking into account the ARI for the BBA DRE and SDRE estimation. Like during the preceding stage, each of the WRF simulations starts with preset global initial conditions. The CHIMERE simulations, performed in parallel, are initialized using concentrations of gaseous and aerosol components found during the first stage. At the very beginning of each six-hour interval, the radiative fluxes are calculated with and without accounting for BBA at nearly the same state of the atmosphere, thereby characterizing DRE. At the same time, these simulations, continued over the time interval τ make it possible to characterize the BBA SDRE (as a function of τ).

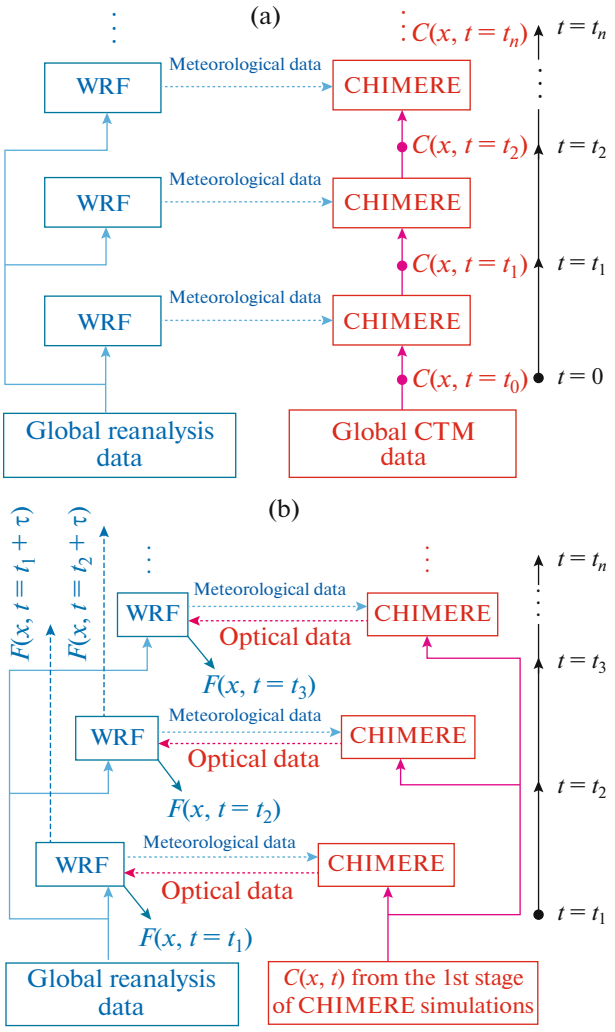

Fig. 1. Schematic representation of the computational technology to estimate the BBA DRE and SDRE using CHIMERE and WRF model simulations: (a) the first (offline) stage of the simulations, outputting the concentrations C of the considered admixtures as functions of coordinates of three-dimensional space x and time t; (b) the second (online) stage of the simulations, outputting spatiotemporal fields of radiative fluxes $F(x, t)$.

Indeed, the difference between meteorological parameters in the considered pairwise online calculations starting with the same initial (meteorological) conditions with and without accounting for the BBA sources is exclusively determined by the counteraction of biomass burning aerosol on meteorological processes. For each time instant and in each model cell, these differences are generally stochastic in character, reflecting the unstable and stochastic properties inher-

ent in atmospheric meteorological processes. However, after these simulations are averaged over space and time, we can identify a stable tendency in the differences between radiative fluxes and, thereby, estimate BBA SDRE.

These simulations during both stages are performed both with and without accounting for the emissions of aerosol and gaseous admixtures from Siberian wildfires. In this work, the time between successive starts of the model $(t_{i+1} - t_i) = 6$ h. The maximal period (τ) of online simulations is 48 h.

The radiative fluxes calculated by the end of each online computer run are used to estimate Φ_{ARI} from Eq. (1). The Φ_d and Φ_{sd} are estimated by Eqs. (2) and (3). The estimates obtained for six-hour counts are averaged over the entire period under study and (if necessary) over the region under study.

We note that, should DRE be exactly calculated, the uncertainties of the SDRE estimates would be primarily associated with the errors in the transport of smoke plumes due to errors in the meteorological forecast performed within the online simulations. Probably, these uncertainties increase in situations with high spatiotemporal variations in smoke density; however, even in these cases, the abovementioned procedure of spatiotemporal averaging of initial estimates favors the reduction of uncertainty of final estimates of radiative effects.

When using the CHIMERE-WRF complex, the Φ_{ARI} can be numerically estimated in an alternative way based directly on successive online simulations, analogous to offline computations during the first stage of the above described technology. In this case, every next WRF run should be initiated using meteorological data calculated in the preceding run; and a procedure of spectral nudging provided in WRF should be used so that meteorological data obtained for a long period would not significantly deviate from reanalysis data [28]. However, this simulation procedure does not allow one to estimate DRE and SDRE separately (which is the aim of the above technology); and the Φ_{ARI} estimates turn out to be dependent on the nudging parameters. A more detailed consideration of this alternative method of estimating the ARI effect is beyond the scope of out work.

2. NUMERICAL EXPERIMENTS

The above-described computational technology was applied in numerical experiments aimed at estimating the radiative effects of Siberian BBA for July 16–31, 2016. This was the period when in Siberia there were large wild fires that caused smoke pollution on the scales of a few thousand kilometers [17, 29]. The simulations mainly used the typical options and parameterizations recommended by CHIMERE developers and described comprehensively in developers' review papers [24, 27], as well in the model documentation (https://www.lmd.polytechnique.fr/chimere/docs/). Below, we briefly describe the configurations of the performed simulations and indicate a number of specific software features which are very significant in the context of the present research.

The simulations were performed on the common CHIMERE/WRF horizontal grid with a resolution of 90 km^2, which covered, in addition to the region of the eastern Arctic (i.e., the region extending poleward of 66.5° N in the Eastern Hemisphere) considered in this work, all Europe and most of Asia (Fig. 2). This coverage allows the simulations to take into account all the main atmospheric pollution sources in the eastern Arctic. In the vertical direction, the CHIMERE and WRF computational grids encompass, respectively, 15 and 33 levels, the uppermost of which correspond to the 200 and 50-hPa pressure levels. The numerical experiments were performed to calculate simultaneously the mass concentrations of particles of smoke, anthropogenic, biogenic, mineral, and marine aerosols. Aerosol particles of all types were divided into 10 ranges of diameters from 10 nm to 40 μm. The dynamics of aerosol particle mass concentration in each of the size ranges was determined by emissions of the primary aerosol, advective and turbulent transport, coagulation, dry and wet deposition, mass exchange in the "gas–particles" system, as well as gas-phase oxidation reactions leading to the formation of the substance of the secondary organic and inorganic aerosols. The concentrations of oxidizers (OH, NO_3, and O_3) were determined by calculating the concentrations of 59 gas admixtures taken into account within the simplified chemical mechanism MELCHIOR2.

In view of unavoidable large uncertainties, inherent in the well-known methods for describing the evolution processes of the organic component of biomass burning aerosol [16–18], and in an attempt to simplify the interpretation of results, in this work we used one of the simplest model representations of organic aerosol (OA) among standard ones in the CHIMERE distribution kit, namely, the representation from [30] corresponding to the configuration parameter soatyp = 2 in the model. Work [30] indicates that the primary OA is composed of nonvolatile organic compounds; and the secondary aerosol is formed in a single-step reaction of few gas-phase pre-

Fig. 2. Spatial distributions of AOD (550 nm) averaged over time (July 16–31, 2016) from (a) model simulations and (b) MODIS satellite measurements; (c) time series of calculated (both with and without accounting for Siberian fires) and measured AOD averaged over the eastern Arctic, and weighted average SSAs (550 nm) in the aerosol column. In panels (a) and (b), the Siberian regions, for which the BBA emissions were optimized is outlined; r is the correlation coefficient between measured and calculated AOD values.

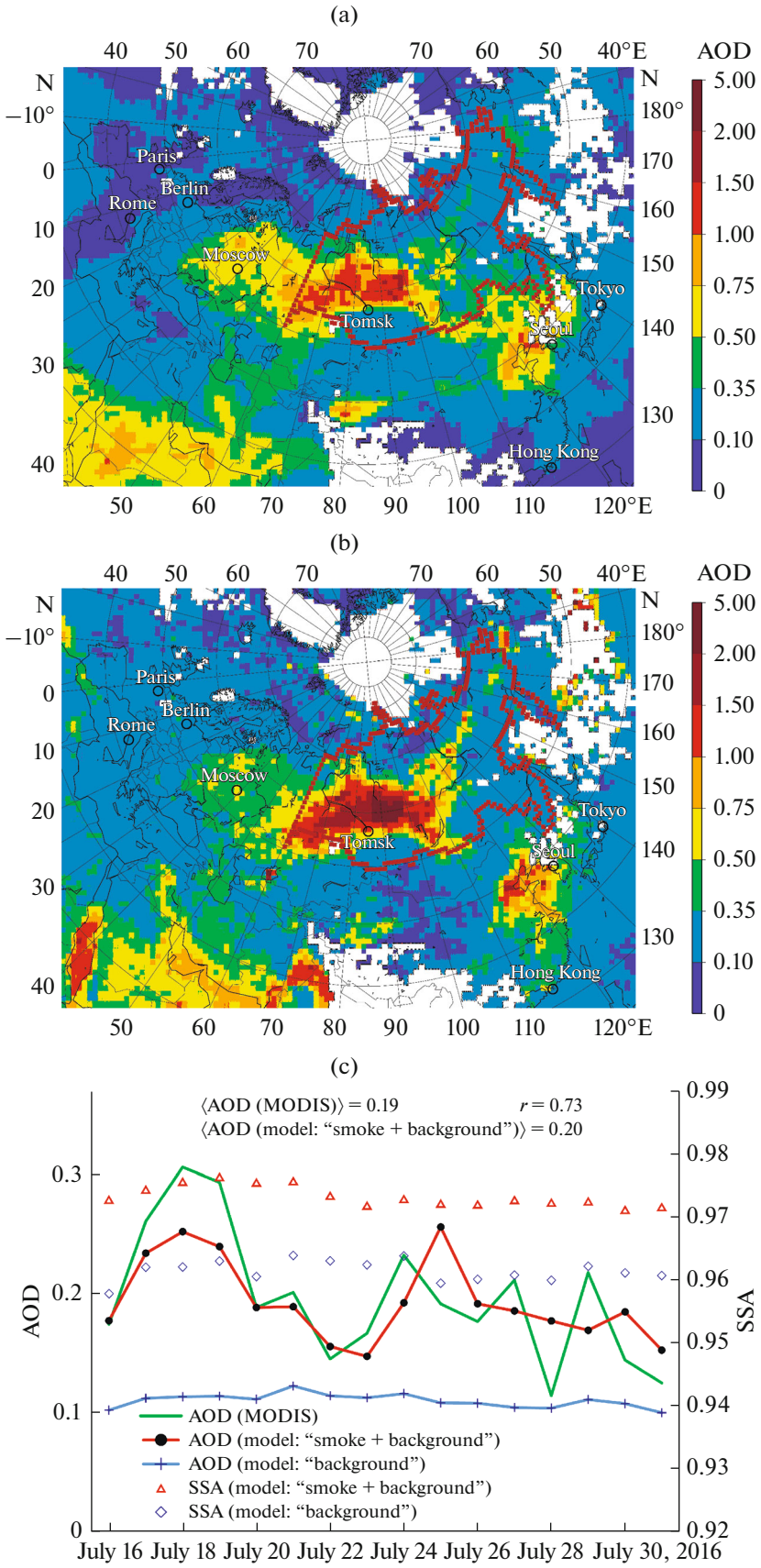
(a)
40 50 60 70 70 60 50 40°E
AOD
N
−10°
0
10
20
30
40
180°
170
160
150
140
130
5.00
2.00
1.50
1.00
0.75
0.50
0.35
0.10
0
Paris
Berlin
Rome
Moscow
Tomsk
Tokyo
Seoul
Hong Kong
50 60 70 80 90 100 110 120°E
(b)
40 50 60 70 70 60 50 40°E
AOD
Paris
Berlin
Rome
Moscow
Tomsk
Tokyo
Seoul
Hong Kong
50 60 70 80 90 100 110 120°E
(c)
⟨AOD (MODIS)⟩ = 0.19
r = 0.73
⟨AOD (model: “smoke + background”)⟩ = 0.20
AOD
SSA
0
0.1
0.2
0.3
0.92
0.93
0.94
0.95
0.96
0.97
0.98
0.99
AOD (MODIS)
AOD (model: “smoke + background”)
AOD (model: “background”)
SSA (model: “smoke + background”)
SSA (model: “background”)
July 16 July 18 July 20 July 22 July 24 July 26 July 28 July 30, 2016

cursors (toluene, tetramethylbenzidine, *n*-butene, and xylene) with the hydroxyl radical (OH), and its components possess low volatility, which can be neglected under the typical conditions in the lower atmosphere. This representation seems to strongly underestimate the formation rate of secondary OA in the initial period (10–15 h into the simulation) of atmospheric evolution of smokes [16, 19]. Siberian smokes can hardly reach the Arctic in the first few hours of their evolution; therefore, the effect of the secondary OA on estimates of BBA radiative effects can be taken into account by increasing OA emissions from Siberian fires. We note that a typical BBA "age" in the Arctic is two days or longer according to estimates within simulations using the "tracer" analysis [17].

In complying with the method developed previously [15], constant correcting factors, f_{OA} and f_{BC}, were applied to "standard" (see discussion below) OA and black carbon emissions, respectively, from Siberian fires. The factor $f_{OA} = 2.2$ satisfies the following condition:

$$\left|\left\langle AOD^{m}\right\rangle - \left\langle AOD^{o}\right\rangle\right|\left\langle AOD^{o}\right\rangle^{-1} < \varepsilon, \qquad (4)$$

where AOD^{m} and AOD^{o} are the calculated and observed AOD values at 550 nm; angular brackets mean the averaging over the eastern Arctic and the period under study, and ε is a small number taken to be 0.03. Satellite data retrieved from MODIS measurements of aerosol were used as observed AOD values [31]. The initial level 2 MODIS data were processed and translated to the model grid, as described previously in works using analogous data [15–17]. The estimate $f_{BC} = 1.5$ was obtained using the ratio of Siberian smoke emissions of black and organic carbon, which was optimized in [15] after the analysis of data from satellite measurements and three-dimensional CHIMERE modeling, with the same simplified OA representation being used as in the present work. Fulfillment of condition (4) is achieved by varying f_{OA} (and f_{BC}, linearly related to the former) during an iteration process [15], which rapidly converges in this situation because the contribution of organic aerosol to AOD^{m} is, on average, dominant (>90%).

The evaluated mass concentrations of aerosol admixtures and preset values of their complex refractive indices were used to calculate the aerosol optical properties (AOD, SSA, and IF) within CHIMERE based on the Mie theory. The absorption of solar radiation by the organic BBA component, i.e., by brown carbon, was taken into account assuming that the imaginary part of refractive index k for all model AO components in smokes from Siberian fires at a given wavelength λ is equal to the same constant value $k_{OA}(\lambda)$ (which power-law depends on λ in UV and visible wavelength ranges) and to zero in the IR spectral range. Based upon the analysis of data from remote sensing of smoke plumes from Siberian fires at AERONET stations [32] and upon laboratory measurements of the optical properties of smokes [33, 34], we have: $k_{OA}(440\ \text{nm}) = 0.0023$, and the exponent of the power-law dependence $k_{OA}(\lambda)$ is -4.0. The value $k_{OA}(388\ \text{nm}) = 0.0038$ calculated according to this dependence is consistent with the analysis of satellite measurements for Siberian smoke plumes that have resided in the illuminated atmosphere for over 20 h [35].

"Standard" (see discussion above) emissions of gas and aerosol admixtures from fires into the atmosphere were specified in each model grid cell with 1-hour resolution using the CAMS-GFAS global database [36]. This database aggregates the estimates of emissions obtained using satellite measurements of the fire radiative power [37]. The hourly anthropogenic emissions of aerosol and gas admixtures were calculated using the CAMS regional anthropogenic emission inventory [38]. The emissions of biogenic, mineral, and marine aerosols were calculated directly by CHIMERE using parameterizations and databases, whose description and validity issues were dealt with in the model documentation and papers [24, 27].

In total, our simulations covered the period from July 1 to 31, 2016, with the first 15 days considered as a transition period and omitted in the subsequent analysis. Data calculated by the LMDz4_INCA3 global climatological model, which are a part of the CHIMERE distribution kit, were used as initial and boundary conditions for the concentrations of gaseous substances and aerosols. The initial and boundary conditions for meteorological parameters were specified using global data from NCEP final reanalysis (https://rda.ucar.edu/).

The simulations were performed using computational technology described in section 1, both with and without accounting for the emissions from Siberian fires. In addition, we performed a test calculation, in which BBA was modeled as a nonabsorbing component (SSA = 1) for the same emissions of primary OA and gas admixtures.

The calculated AOD values are compared with satellite measurements in Fig. 2. In particular, we can note that the regions of increased AOD in Western Siberia and in European Russia stand out in the spatial distributions of both calculated and measured AODs (see Figs. 2a and 2b), the origin of which was shown previously [17] to be due to Siberian fires. The model underestimates the AOD in Western Siberia, nonetheless looking realistically on the whole. The model adequately reproduces the mean level and a considerable part of time variations in the retrieved AOD in the eastern Arctic (see Fig. 2c). Although the validation of the model SSA simulations is beyond the scope of the present work, the calculated values of this important characteristic (see Fig. 2c) are quite high ($\sim$ 0.91–0.99) and close to those typical for boreal smokes [32, 39].

Table 1. Radiative effects (W m^{-2}) of Siberian BBA at the top (TOA) and bottom of the atmosphere (BOA) averaged over time (July 16–31, 2016) and space (over the entire eastern Arctic or only over a part of its territory covered by ice or snow)

Radiative effect	Eastern Arctic		Snow-ice surface	
	TOA	BOA	TOA	BOA
DRE	−6.0/−6.7	−6.7/−5.4	−1.2/−2.7	−2.0/−1.4
SDRE	2.0/1.9	1.8/1.5	1.6/1.6	1.2/0.9
ARI	−4.0/−4.8	−4.9/−3.9	0.4/−1.1	−0.8/−0.5

Entries before and after slash are calculated, respectively, with and without accounting for absorbing components in the composition of Siberian smokes.

3. RESULTS OF NUMERICAL EXPERIMENTS

Based on the model simulations in accordance with computational technology suggested here (see section 1), we estimated the direct and semidirect effects (Φ_d and Φ_{sd}), as well as the total ARI effect (Φ_{ARI}) of Siberian biomass burning aerosol in each model grid cell for July 16–31, 2016, taking into account the radiative fluxes in UV, visible, and IR spectral ranges. The spatial distributions of the values of these effects at the top of the atmosphere averaged over the period specified are shown in Fig. 3. The spatially averaged radiative effects, pertaining only to the region of the eastern Arctic, are presented in Table 1. They correspond to $\tau = 48$ h (see section 1).

The spatial distribution of the DRE estimates (Fig. 3a) shows that the DRE is negative in almost all the simulation domain. In other words, Siberian smokes mainly cool the atmosphere, primarily because scattering of incoming solar radiation by weakly absorbing aerosol particles predominates over its absorption. The DREs, largest in absolute value (>30 W m^{-2}), were obtained over the territory of Western Siberia, where smoke plumes were the densest (see Figs. 2a and 2b). A significant, though much weaker, BBA radiative effect (>5 W m^{-2} in absolute value) is also manifested over a substantial part of the eastern Arctic. The DRE of Siberian BBA at the top of the atmosphere averaged over the entire eastern Arctic is −6.0 W m^{-2} (Table 1). The cooling effect of BBA is even stronger at the bottom of the atmosphere (−6.7 W m^{-2}), in particular, because a portion of solar radiation is absorbed by black and brown carbon in the atmospheric depth. When there is no black and brown carbon in the BBA composition, the DRE increases (decreases) in absolute value at the top (bottom) of the atmosphere. On the whole, the presence of absorbing components in BBA composition in the eastern Arctic offsets only a little more than 10% of the cooling effect of BBA, which is determined by scattering components. The role of black and brown carbon is much more significant over the snow-ice cover of the ocean, where these components offset more than a half of the cooling BBA effect (which is known to weaken over surfaces with a high reflectance). We note that the predominance of negative DRE values of BBA in the Arctic, revealed in the abovementioned model simulations, is consistent with the previous observation-based analysis [6], however, not going quite hand in hand with certain model studies [9, 11].

In contrast to DRE, the SDRE values are predominantly positive (see Fig. 3b). They are much smaller than the corresponding DRE in absolute value, but comparable in the order of magnitude. On the average over the entire eastern Arctic, SDRE offsets approximately 30% of DRE, indicating the significance of this effect in the context of the problem of estimating the ARI effects in the Arctic. The role of the BBA SDRE is most significant over snow-ice covered surfaces. In this case, the semidirect effect exceeds the direct effect in absolute value and leads to the positive ARI effect (0.4 W m^{-2}). The region of positive values of the ARI effect poleward of polar circle is highlighted in Fig. 3c as a large yellow spot northward of 70° N and largely coincides with the region of ice cover that persisted in the Arctic into late July 2016. We note that the radiative balance in the Arctic is especially important to know over snow-ice surfaces because its changes can either speed up or slow down the reduction of the snow cover and, in particular, as a consequence of the "ice–albedo" feedback [40]. In this context, the simulations, performed in this work, indicate that SDRE should be considered, in addition to the radiative effects of black carbon depositions, as a significant factor acting to increase the Arctic atmospheric temperature.

As was already indicated above, the estimates of the SDRE and of the ARI effect, presented in Fig. 3 and in Table 1, were obtained for a fixed duration of radiation effect of Siberian BBA on the meteorology ($\tau = 48$ h). At the same time, it was assumed (see section 1) that, although these SDRE estimates depend on τ in the general case, this dependence is close to saturating; therefore, the choice of a specific (but quite a large) τ does not matter much. The validity of this assumption is confirmed by simulations in Fig. 4, which shows $\Phi_{sd}(\tau)$ and $\Phi_{ARI}(\tau)$ averaged over the eastern Arctic, and, in particular, those separately calculated over different surface types.

The $\Phi_{sd}(\tau)$ and $\Phi_{ARI}(\tau)$ grow most strongly for first 10–15 h of the atmosphere adaption to the aerosol

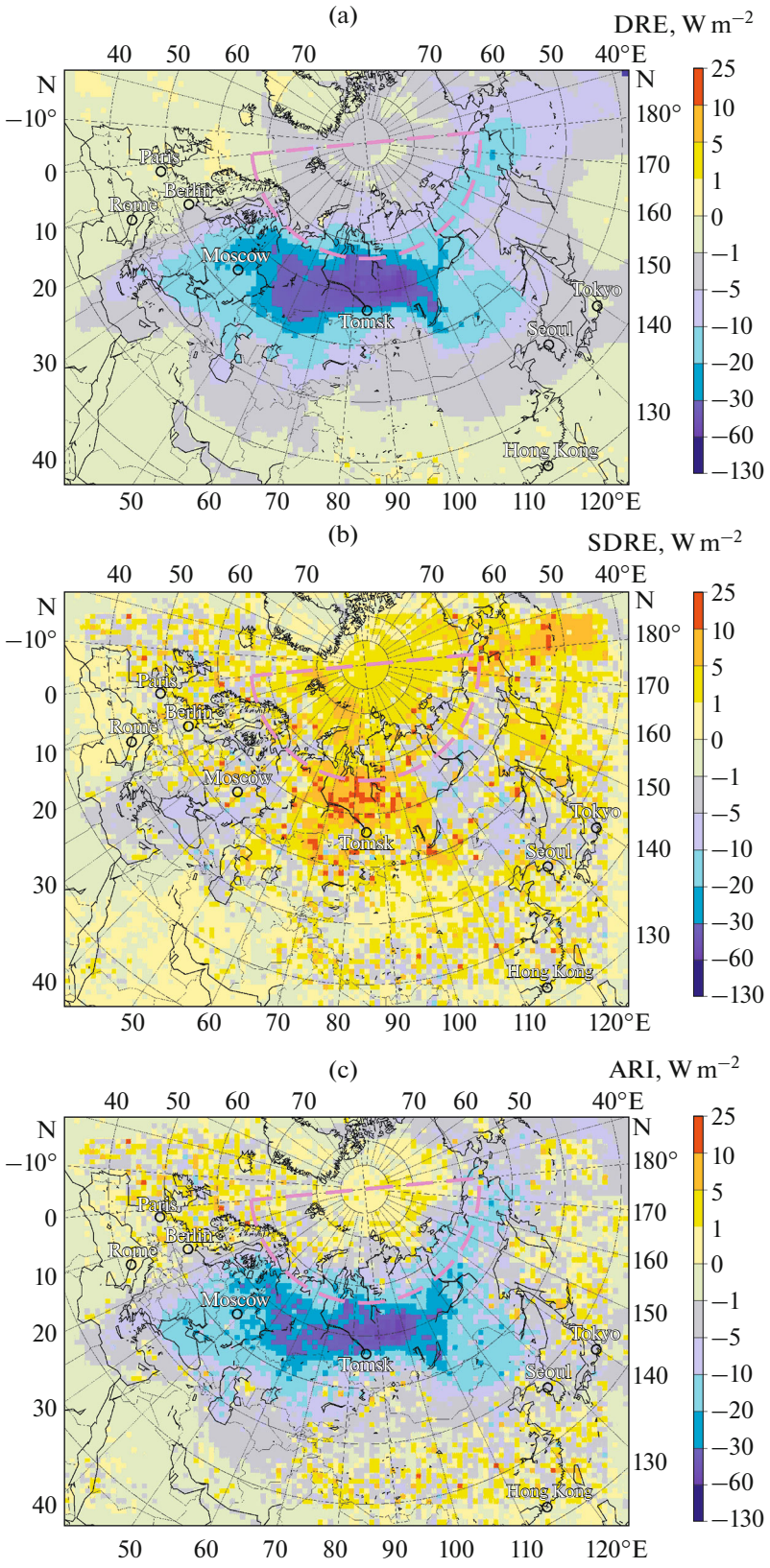

Fig. 3. Spatial distributions of (a) DRE and (b) SDRE averaged over the period under study (July 16–31, 2016), as well as of (c) the total ARI of Siberian BBA (W m^{-2}) at the top of the atmosphere. Dashed curves show the region of the eastern Arctic.

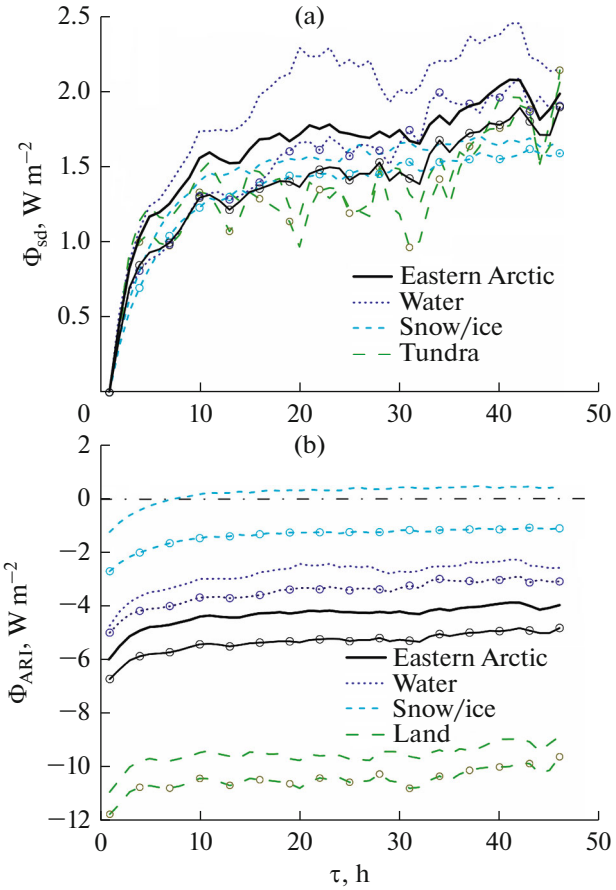

Fig. 4. Dependences of (a) semidirect and (b) total radiative effects of Siberian BBA at the top of the atmosphere on the duration of radiative effect of smokes in our numerical experiments. Shown are the radiative effects averaged over the entire territory of the eastern Arctic, as well as separately over territories corresponding to three different surface types inside the same region. Circles mark the dependences plotted using simulations without accounting for absorbing components in the composition of Siberian smokes.

forcing. Then, these quantities show slower and largely irregular fluctuations, seemingly reflecting the complex dependence of the BBA SDRE evolution on specific meteorological conditions and indicating the corresponding uncertainties in the SDRE estimates derived. The uncertainties can be reduced after the radiative characteristics are averaged over a period as long as possible, with aerosol forcing kept unchanged, which is hardly feasible without multiyear climatic simulations. Nonetheless, despite the fact that the SDRE dependence on τ indicates considerable uncertainties of the our estimates, the results in Fig. 4 argue quite convincingly that the BBA effect on the meteorological properties in this period of time is offset to some degree the DRE-caused cooling effect of BBA.

Analysis of the ways of SDRE formation in smokes from Siberian fires, which was singled out for the first time in this research, is beyond the scope of this work. Seemingly, these qualitatively differ from SDRE formation of atmospheric aerosol studied (or suggested) before. Indeed, the semidirect radiative effect of atmospheric aerosol is traditionally associated with heating of the atmosphere due to the absorption of solar radiation by black carbon [3, 20, 21, 41, 42]. However, the test simulations, performed without accounting for absorbing components in the composition of Siberian BBA (see dependences highlighted by circles in Fig. 4) indicate that, in the absence of aerosol absorption, SDRE not only survives, but insignificantly decreases as compared to the base calculation. In this regard, we hypothesize that SDRE can be formed due to the decrease in the optical depth of the middle- and upper-level clouds owing to weakening of the vertical moisture flux, which, in turn, occurs in response to the cooling of air because of aerosol scattering and to the acceleration of water vapor condensation in the surface air layer. Justification of this hypothesis and clarification of the role the SDRE of Siberian BBA plays in climate-forming processes in the Arctic, requires further studies.

CONCLUSIONS

We describe the first experience of applying the complex of regional models, comprising the Chemistry Transport Model (CTM) CHIMERE and meteorological model WRF, to studying the radiative effects of Siberian BBA in the Arctic. An original technology of numerical experiments, based on the model complex CHIMERE-WRF, is presented with the purpose of estimating the BBA DRE and SDRE. Certain capabilities of this model complex and of developed computational technology in studying how smokes from Siberian fires influence the radiative balance of the atmosphere in the eastern Arctic are demonstrated by the example of numerical experiments covering the period from July 16 to 31, 2016.

Our simulations showed that Siberian BBA in that period of time had a strong cooling effect on the atmosphere in the eastern Arctic through DRE, the value of which at the top of the atmosphere was -6.0 W m^{-2} on average. The calculated spatial distribution of the Siberian BBA DRE demonstrates that this effect weakens (in absolute value) with decreasing distance to the North Pole.

At the same time, our results indicate that the contribution of the Siberian BBA DRE to the radiative balance in the eastern Arctic is offset to a certain degree by SDRE, associated with the BBA counteraction on meteorological process (and, in particular, on clouds). Model estimates indicate that the Siberian BBA SDRE, on average, is positive (i.e., leads to atmospheric warming) and amounts to ~2 W m^{-2}. The role of SDRE is most significant over snow-ice surfaces, where it exceeds DRE in absolute value, thus leading to the positive total radiative effect of Siberian

BBA (~0.4 W m^{-2}). The processes causing the occurrence of the Siberian BBA SDRE in the Arctic are argued to be qualitatively different from previously known formation processes of the atmospheric aerosol SDRE. A more detailed consideration of these processes should be the subject of future studies.

FUNDING

The study of the direct radiative effect of Siberian smokes was supported by the Russian Science Foundation (grant no. 19-77-20109). The simulation of the semidirect radiative effect of Siberian biomass burning aerosol was supported by the Russian Foundation for Basic Research (grant no. 21-55-15009).

CONFLICT OF INTEREST

The authors declare that they have no conflicts of interest.

OPEN ACCESS

REFERENCES

1. M. Sand, T. Berntsen, K. von Salzen, M. Flanner, J. Langner, and D. Victor, "Response of Arctic temperature to changes in emissions of short-lived climate forcers," Nat. Climate Change **6**, 286–289 (2016).
2. N. Bellouin, O. Boucher, J. Haywood, and M. Shekar Reddy, "Global estimate of aerosol direct radiative forcing from satellite measurements," Nature **438**, 1138–1141 (2005).
3. J. Hansen, M. Sato, and R. Reudy, "Radiative forcing and climate response," J. Geophys. Res. **102**, 6831–6864 (1997).
4. S. Twomey, "The Influence of pollution on the shortwave albedo of clouds," J. Atmos. Sci. **34**, 1149–1152 (1977).
5. J. Hansen and L. Nazarenko, "Soot climate forcing via snow and ice albedos," Proc. Natl. Acad. Sci. USA **101** (2), 423–428 (2004).
6. N. Evangeliou, Y. Balkanski, W. M. Hao, A. Petkov, R. P. Silverstein, R. Corley, B. L. Nordgren, S. P. Urbanski, S. Eckhardt, A. Stohl, P. Tunved, S. Crepinsek, A. Jefferson, S. Sharma, J. K. Nojgaard, and H. Skov, "Wildfires in Northern Eurasia affect the budget of black carbon in the Arctic—a 12-year retrospective synopsis (2002—2013)," Atmos. Chem. Phys. **16**, 7587–7604 (2016).
7. T. B. Zhuravleva, I. M. Nasrtdinov, and A. A. Vinogradova, "Direct radiative effects of smoke aerosol in the region of Tiksi Station (Russian Arctic): Preliminary results," Atmos. Ocean. Opt. **32** (3), 296–305 (2019).
8. J. Lisok, A. Rozwadowska, J. G. Pedersen, K. M. Markowicz, C. Ritter, J. W. Kaminski, J. Struzewska, M. Mazzola, R. Udisti, S. Becagli, and I. Gorecka, "Radiative impact of an extreme arctic biomass-burning event," Atmos. Chem. Phys. **18**, 8829–8848 (2018).
9. L. M. Zamora, R. A. Kahn, S. Eckhardt, A. McComiskey, P. Sawamura, R. Moore, and A. Stohl, "Aerosol indirect effects on the nighttime Arctic ocean surface from thin, predominantly liquid clouds," Atmos. Chem. Phys. **17**, 7311–7332 (2017).
10. M. G. Tosca, J. T. Randerson, and C. S. Zender, "Global impact of smoke aerosols from landscape fires on climate and the hadley circulation," Atmos. Chem. Phys. **13**, 5227–5241 (2013).
11. Y. Jiang, Z. Lu, X. Liu, Y. Qian, K. Zhang, Y. Wang, and X.-Q. Yang, "Impacts of global open-fire aerosols on direct radiative, cloud and surface-albedo effects simulated with CAM5," Atmos. Chem. Phys. **16**, 14805–14824 (2016).
12. M. Sand, B. H. Samset, Y. Balkanski, S. Bauer, N. Bellouin, T. K. Berntsen, H. Bian, M. Chin, T. Diehl, R. Easter, S. J. Ghan, T. Iversen, A. Kirkevag, J.-F. Lamarque, G. Lin, X. Liu, G. Luo, G. Myhre, T. V. Noije, J. E. Penner, M. Schulz, O. Seland, R. B. Skeie, P. Stier, T. Takemura, K. Tsigaridis, F. Yu, K. Zhang, and H. Zhang, "Aerosols at the poles: An AeroCom Phase II multi-model evaluation," Atmos. Chem. Phys. **17**, 12197–12218 (2017).
13. X. Wang, C. L. Heald, J. Liu, R. J. Weber, P. Campuzano-Jost, J. L. Jimenez, J. P. Schwarz, and A. E. Perring, "Exploring the observational constraints on the simulation of brown carbon," Atmos. Chem. Phys. **18**, 635–653 (2018).
14. D. S. Hamilton, S. Hantson, C. E. Scott, J. O. Kaplan, K. J. Pringle, L. P. Nieradzik, A. Rap, G. A. Folberth, D. V. Spracklen, and K. S. Carslaw, "Reassessment of pre-industrial fire emissions strongly affects anthropogenic aerosol forcing," Nat. Commun. **9**, 3182 (2018).
15. I. B. Konovalov, D. A. Lvova, M. Beekmann, H. Jethva, E. F. Mikhailov, J.-D. Paris, B. D. Belan, V. S. Kozlov, P. Ciais, and M. O. Andreae, "Estimation of black carbon emissions from Siberian fires using satellite observations of absorption and extinction optical depths," Atmos. Chem. Phys. **18**, 14889–14924 (2018).
16. I. B. Konovalov, M. Beekmann, E. V. Berezin, P. Formenti, and M. O. Andreae, "Probing into the aging dynamics of biomass burning aerosol by using satellite measurements of aerosol optical depth and carbon monoxide," Atmos. Chem. Phys. **17**, 4513–4537 (2017).
17. I. B. Konovalov, N. A. Golovushkin, M. Beekmann, and M. O. Andreae, "Insights into the aging of biomass burning aerosol from satellite observations and 3D atmospheric modeling: Evolution of the aerosol optical properties in Siberian wildfire plumes," Atmos. Chem. Phys. **21** (1), 357–392 (2021).
18. I. B. Konovalov, M. Beekmann, N. A. Golovushkin, and M. O. Andreae, "Nonlinear behavior of organic aerosol in biomass burning plumes: A microphysical

model analysis," Atmos. Chem. Phys. **19** (19), 12091–12119 (2019).

19. T. Zhuravleva, I. Nasrtdinov, I. Konovalov, N. Golovushkin, and M. Beekmann, "Impact of the atmospheric photochemical evolution of the organic component of biomass burning aerosol on its radiative forcing efficiency: A box model analysis," Atmosphere **12**, 1555 (2021).
20. J. D. Lindeman, Z. Boybeyi, and I. Gultepe, "An examination of the aerosol semi-direct effect for a polluted case of the ISDAC field campaign," J. Geophys. Res. **116**, T10 (2011).
21. E. Stofferahn and Z. Boybeyi, "Investigation of aerosol effects on the arctic surface temperature during the diurnal cycle: Part 2—Separating aerosol effects," Int. J. Climatol. **37**, 775–787 (2017).
22. Z. Lu and I. N. Sokolik, "Examining the impact of smoke on frontal clouds and precipitation during the 2002 Yakutsk wildfires using the WRF-Chem-SMOKE model and satellite data," J. Geophys. Res.: Atmos. **122**, 12765–12785 (2017).
23. J. C. Pere, B. Bessagnet, M. Mallet, F. Waquet, I. Chiapello, F. Minvielle, V. Pont, and L. Menut, "Direct radiative effect of the Russian wildfires and its impact on air temperature and atmospheric dynamics during August 2010," Atmos. Chem. Phys. **14**, 1999–2013 (2014).
24. L. Menut, B. Bessagnet, D. Khvorostyanov, M. Beekmann, N. Blond, A. Colette, I. Coll, G. Curci, G. Foret, A. Hodzic, S. Mailler, F. Meleux, J.-L. Monge, I. Pison, G. Siour, S. Turquety, M. Valari, R. Vautard, and M. G. Vivanco, "CHIMERE 2013: A model for regional atmospheric composition modeling," Geosci. Model Dev. **6**, 981–1028 (2013).
25. P. Tuccella, L. Menut, R. Briant, A. Deroubaix, D. Khvorostyanov, S. Mailler, G. Siour, and S. Turquety, "Implementation of aerosol-cloud interaction within WRF-CHIMERE online coupled model: Evaluation and investigation of the indirect radiative effect from anthropogenic emission reduction on the Benelux Union," Atmosphere **10**, 20 (2019).
26. R. Briant, P. Tuccella, A. Deroubaix, D. Khvorostyanov, L. Menut, S. Mailler, and S. Turquety, "Aerosol-radiation interaction modelling using online coupling between the WRF 3.7.1 meteorological model and the CHIMERE 2016 chemistry-transport model, through the OASIS3-MCT coupler," Geosci. Model Dev. **10**, 927–944 (2017).
27. L. Menut, B. Bessagnet, R. Briant, A. Cholakian, F. Couvidat, S. Mailler, R. Pennel, G. Siour, P. Tuccella, S. Turquety, and M. Valari, "The CHIMERE V2020r1 online chemistry-transport model," Geosci. Model Dev. **14**, 6781–6811 (2021).
28. G. Miguez-Macho, G. L. Stenchikov, and A. Robock, "Spectral nudging to eliminate the effects of domain position and geometry in regional climate model simulations," J. Geophys. Res. Atmos. **109** (D13104), 1–14 (2004).
29. G. I. Gorchakov, G. S. Golitsyn, S. A. Sitnov, A. V. Karpov, I. A. Gorchakova, R. A. Gushchin, and O. I. Datsenko, "Large-scale haze over Eurasia in July 2016," Dokl. Earth Sci. **482** (1), 1212–1215 (2018).
30. B. Bessagnet, L. Menut, G. Curci, A. Hodzic, B. Guillaume, C. Liousse, S. Moukhtar, B. Pun, C. Seigneur, and M. Schulz, "Regional modeling of carbonaceous aerosols over Europe—focus on secondary organic aerosols," J. Atmos. Chem. **61**, 175–202 (2009).
31. R. C. Levy, S. Mattoo, L. A. Munchak, L. A. Remer, A. M. Sayer, F. Patadia, and N. C. Hsu, "The Collection 6 MODIS aerosol products over land and ocean," Atmos. Meas. Tech. **6**, 2989–3034 (2013).
32. I. B. Konovalov, N. A. Golovushkin, M. Beekmann, M. V. Panchenko, and M. O. Andreae, "Inferring the absorption properties of organic aerosol in Siberian biomass burning plumes from remote optical observations," Atmos. Meas. Tech. **14**, 6647–6673 (2021).
33. C. D. McClure, C. Y. Lim, D. H. Hagan, J. H. Kroll, and C. D. Cappa, "Biomass-burning-derived particles from a wide variety of fuels—Part 1: Properties of primary particles," Atmos. Chem. Phys. **20**, 1531–1547 (2021).
34. V. S. Kozlov, I. B. Konovalov, M. V. Panchenko, V. P. Shmargunov, and E. P. Yausheva, "Dynamics of aerosol absorption characteristics in smoke combustion of forest biomass burning at the large aerosol chamber at the stages of generation and aging in time," Proc. SPIE—Int. Soc. Opt. Eng. **11916**, 119164 (2021).
35. I. B. Konovalov, N. A. Golovushkin, M. Beekmann, and S. Turquety, "Using multi-platform satellite observations to study the atmospheric evolution of brown carbon in siberian biomass burning plumes," Remote Sens. **14**, 2625 (2022).
36. CAMS—the Copernicus Atmosphere Monitoring Service team: Global Fire Assimilation System v2.1, Fire Radiative Power, ECMWF. http://apps.ecmwf.int/datasets/data/cams-gfas. Cited May 14, 2022.
37. J. W. Kaiser, A. Heil, M. O. Andreae, A. Benedetti, N. Chubarova, L. Jones, J.-J. Morcrette, M. Razinger, M. G. Schultz, M. Suttie, and G. R. van der Werf, "Biomass burning emissions estimated with a global fire assimilation system based on observed fire radiative power," Biogeosci **9**, 527–554 (2012).
38. H. van der Gon, J. Doubalova, N. Elguindi, B. Galle, M. Gauss, M. Guevara, J.-P. Jalkanen, J. Kuenen, C. Liousse, B. Quack, D. Simpson, and K. Sindelarova, The Copernicus Atmosphere Monitoring Service Global and Regional Emissions (April 2019 Version) (Copernicus Atmosphere Monitoring Service, 2019). https://doi.org/10.24380/d0bn-kx16
39. N. Chubarova, Ye. Nezval', I. Sviridenkov, A. Smirnov, and I. Slutsker, "Smoke aerosol and its radiative effects during extreme fire event over Central Russia in summer 2010," Atmos. Meas. Tech. **5**, 557–568 (2012).
40. K. Pistone, I. Eisenman, and V. Ramanathan, "Radiative heating of an ice-free Arctic Ocean," Geophys. Rev. Lett. **46**, 7474–7480 (2019).
41. R. J. Allen, A. Amiri-Farahani, J. F. Lamarque, C. Smith, D. Shindell, T. Hassan, and C. E. Chung, "Observationally constrained aerosol-cloud semi-direct effects," Clim. Atmos. Sci. **2**, 16 (2019).
42. M. Mallet, F. Solmon, P. Nabat, N. Elguindi, F. Waquet, D. Bouniol, A. M. Sayer, K. Meyer, R. Roehrig, M. Michou, P. Zuidema, C. Flamant, J. Redemann, and P. Formenti, "Direct and semi-direct radiative forcing of biomass-burning aerosols over the southeast Atlantic (SEA) and its sensitivity to absorbing properties: A regional climate modeling study," Atmos. Chem. Phys. **20**, 13191–13216 (2020).

Translated by O. Bazhenov